Thermal evolution of porous anodic aluminas: a comparative study

M.E. Mata-Zamora and J.M. Saniger
Centro de Ciencias Aplicadas y Desarrollo Tecnológico, Universidad Nacional Autónoma de México, Apartado Postal 70-186, México, 04510 D.F.,
e-mail: zamat@aleph.cinstrum.unam.mx, saniger@aleph.cinstrum.unam.mx

Recibido el 23 de mayo de 2005; aceptado el 7 de julio de 2005

The comparative study presented in this work concerning the thermal evolution of sulfuric, oxalic and phosphoric porous anodic aluminas, points out some differences among their physico-chemical and structural properties which were not previously reported. Empirical formulas calculated from the thermal analysis of all the anodic aluminas under study indicate that sulfuric aluminas have a significant higher content of dopant anionic species, oxygen excess, and hydroxyl groups than the oxalic and phosphoric aluminas, indicating that porous sulfuric anodic aluminas should have a higher structural disorder and hydrophilic character than its counterparts. For all samples, transition alumina phases are formed around 900°C and α-alumina above 1200°C, but in these transformations sulfuric and oxalic aluminas follow a different evolution from phosphoric alumina. In the former case, the formation of transition aluminas occurs with the almost simultaneous thermal decomposition of sulfates and oxalates and finally a pure α-Al_2O_3 phase is formed; while for the phosphoric alumina, the phosphate does not decompose even at 1400°C, when a α-Al_2O_3phase unpurified with $AlPO_4$ is observed. Infrared spectroscopy studies show that the coordination modes of the sulfuric and oxalic dopant species start to change well before their thermal decomposition, while, in the case of the phosphoric alumina, aluminum phosphate starts to form at the same time as the transition alumina phases.

Keywords: Anodic porous alumina; nanostructures; thermal analysis.

En este trabajo se presenta un estudio comparativo de la evolución térmica de las alúminas porosas anódicas sulfúrica, oxálica y fosfórica que evidencia diferencias importantes en sus propiedades físico-químicas no reportadas previamente. Las fórmulas empíricas calculadas a partir del análisis térmico de cada tipo de alúmina demuestran que la alúmina anódica sulfúrica tiene un contenido significativamente mayor que la oxálica y fosfórica en cuanto a especies aniónicas dopantes, grupos hidroxilos y oxígeno en exceso, lo que implica que esta alúmina anódica porosa debe tener un mayor carácter hidrofílico y mayor desorden estructural que sus contrapartes. Para los tres tipos de alúminas anódicas porosas en estudio, las fases cristalinas, conocidas genéricamente como alúminas de transición, se forman alrededor de los 900°C y la fase estable de α-alúmina se forma por encima de los 1200°C. Sin embargo, durante la evolución térmica, se observa un comportamiento de la alúmina fosfórica claramente diferenciable del de las alúminas sulfúricas y oxálicas. Para el caso de éstas últimas, la formación de las alúminas de transición ocurre de manera casi simultánea con la descomposición térmica de los sulfatos y oxalatos incorporados a la matriz de la alúmina que se liberan finalmente en forma de SO_2 y CO_2, mientras que para el caso de la alúmina fosfórica los fosfatos incorporados a la matriz no se descomponen térmicamente aún después de calentar las muestras a 1400°C, sino que se segregan de la matriz de alúmina formando una fase de $AlPO_4$ que permanece junto con la fase mayoritaria de α-Al_2O_3. Los estudios por espectroscopía infrarroja muestran que los modos de coordinación de los sulfatos y oxalatos incorporados a la matriz de alúmina porosa comienzan a cambiar bastante antes de su descomposición térmica y liberación, mientras que en el caso de la alúmina fosfórica, se observan indicios del inicio de la formación del fosfato de aluminio de manera coincidente con la formación de las alúminas de transición.

Descriptores: Alúmina anódica porosa; nanoestructuras; análisis térmico.

PACS: 82.45.Cc; 81.16.Pr; 81.70.Pg

1. Introduction

Porous Anodized Aluminum Oxide (AAO) has been known since the beginning of the twentieth century [1] for its high-tech importance in the industrial anodization of aluminum. More recently, due to its ideal nanopore geometrical arrangement, it was proposed as a promising template for the growth of 1D arrays [2-4] such us bundles of nanotubes or nanowires, which constitutes a critical step in the development of operative nanodevices. In fact, AAO porous templates with densities ranging from 10^9-10^{11} pores/cm^2, diameters between 15 and 150 nm, and pore aspect ratios typically ranging from 10 to 1000 [5-7], are routinely prepared following well established techniques.

In the last few a years a significant number of papers have been published reporting the growth of carbon nanotubes [8-10], metallic nanowires, oxide and chalcogenide semiconductor nanowires [11-15], etc, inside the porous AAO templates. In most of these works the porous AAO films are considered simply as mechanically inert supports, ready to be filled using a variety of techniques such as the pyrolysis of hydrocarbon compounds, AC-electrochemical deposition or immersion in colloidal suspensions. This approach works reasonably well for many cases, but it does not take into account the specific chemical composition and properties of the pore walls, which could play an important role in the definition of alternative synthetic routes for the preparation of a variety of new 1D structures. In this sense, some authors have noted that the pore walls seem to be active in processes such as the pyrolysis of hydrocarbons [16-18], ammonia sensing, and pyrene derivatives chemisorption layer onto porous alumina [19-20].

On the other hand, several works have been published about the physico-chemical characterization of anodic alumina pore walls [21-24]; nevertheless, this information is spread throughout different papers, and a comprehensive information of the subject is difficult to obtain from them. In this context, we present in this work a detailed comparative study of the thermal evolution of sulfuric, oxalic and phosphoric porous anodic aluminas, supported with their X-ray diffractograms and infrared spectra obtained in a wide temperature interval, in order to show the different properties of each kind of anodic aluminas, emphasizing the distinctive behavior of phosphoric alumina, which has not previously been reported. This study provides an increase in the understanding of the role played by the anionic species in the thermal transformation of porous anodic aluminas, which should be useful for future modification of the chemical functionality of the anodic porous aluminas.

2. Experiment

High purity aluminum (99.999%) foils with a thickness of 0.13 mm were used as starting material. Prior to anodization, the aluminum was annealed under air at 480°C for 60 minutes. The annealed plates of 10 mm $\times$ 25 mm were electrochemically polished (1:5 v/v of EtOH/$HClO_4$) and then mounted as the anode in an electrochemical cell, using a graphite cathode. The preparation of the sulfuric, oxalic and phosphoric anodic porous aluminas was carried out using the standard condition reported in the literature [5,6]: 0.3 M oxalic acid at 40 V for oxalic aluminas; 0.3 M sulfuric acid at 20 V for sulfuric aluminas; and 0.4 M phosphoric acid at 100 V for phosphoric aluminas. The temperature bath was kept at 10°C, and anodization time was changed as a function of the desired thickness of AAO films. In order to obtain separated aluminum oxide films, the aluminum substrate was eliminated by electrochemical etching in 20 wt% HCl solution, with an operating voltage between 1-5 V. Figure 1 shows images AFM of pore array of sulfuric, oxalic and phosphoric porous alumina films.

Thermoanalysis was carried out with a NETZSCH simultaneous TGA and DSC thermal analyzer, model Jupiter® STA 449. The samples were prepared from pieces of the alumina films milled in agata mortar. A sample mass of 30 mg, alumina crucible, a heating rate of 10°C/min. from room temperature to 1450°C, and dynamic air atmosphere (50 mL/min of air as carrier gas, 10 mL/min of N_2 as protective gas) were the experimental parameters for all the tests.

The infrared spectra of the films were obtained with a Nicolet-5SX Fourier transform spectrophotometer using a TGS detector at a resolution of 4 cm^{-1}. The spectra were recorded from two different kinds of samples:

a) as-prepared substrate-free alumina films (grown for 3.5 hours) to study the absorption bands of the dopant anionic species;

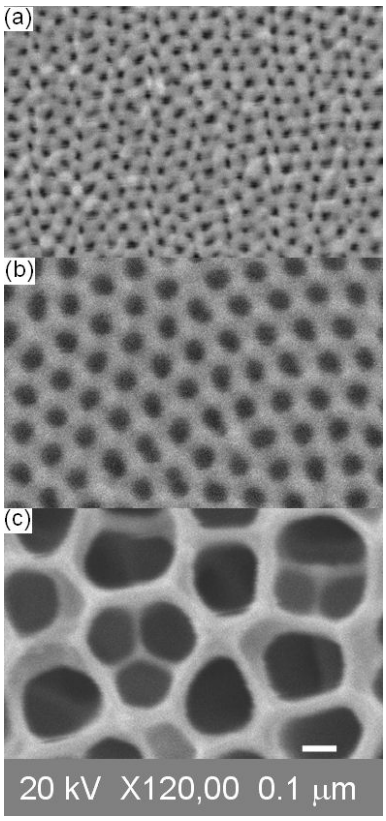

FIGURE 1. SEM micrographs of the bottom view of anodic alumina films. (a) sulfuric; (b) oxalic; and (c) phosphoric anodic aluminas.

b) standard KBr pellets to study the characteristic Al-O vibrations bands and the evolution of dopant species above 800°C for the phosphoric alumina.

The X-ray diffractograms were obtained using a Siemens D-5000 diffractometer with Cu $K_{\alpha 1}$ radiation at 30 KV, a step size of 0.04° during 20 s.

A semiquantitative determination of the aluminum/phosphorous ratio of the phosphoric anodic aluminas was made by X-ray fluorescence, by diluting 50 mg of the alumina sample in 3 g of SiO_2in order to prepare a suitable pellet for the analytical determination. The equipment used was an FRX Siemens SR300.

3. Summary of previous work

It is generally accepted [25] that the walls of the AAO pores have an amorphous structure and that they are formed by the aggregation of nanoparticles with sizes ranging from 2.5 to 4 nm. In addition, porous AAO films present an important number of dopant anionic species inserted into the alumina matrix [26-29], which come from the anodization electrolytes used; so oxalate anions are present in the porous AAO films prepared with oxalic acid electrolyte, while sulfates or phosphates are found in the samples prepared with sulfuric or phosphoric acids, respectively. The presence and

distribution of these dopant species in the pore walls have been studied [28,29], showing that their concentration is not uniform along the wall thickness; their maximum is located between the middle of the wall and the external side [26,28]. The amount of anionic species incorporated depends on their concentration in the electrolyte as well as on the anodization current density, nevertheless a quantification of their relative concentration under any specific preparation conditions has not been presented in the papers consulted.

With respect to their structural units, NMR studies have shown that amorphous porous anodized aluminas are formed by tetra and hexacoordinated aluminum (AlO_4 and AlO_6 polyhedral units) resembling the microstructure of transition aluminas, but an important fraction of pentacoordinated aluminum (AlO_5 polyhedra) is also present [28]. The surface texture of the AAO is also an interesting feature of these materials [24]; the original amorphous samples have a low specific area (about 9 m^2/g), which increases notably (around 100 m^2/g) when heated to the transition temperature for γ, η or θ-alumina. Thermal analysis results of sulfuric and oxalic AAO have also been published [23,24], but they were limited merely to the determination of the transition temperatures; thermal analysis of the phosphoric anodic alumina was not found in the literature consulted.

4. Results

4.1. Infrared spectroscopic characterization of original samples

Figure 2 shows the infrared spectra of representative as-prepared sample films. The broad and intense band centered at 3400 cm^{-1}, characteristic of the OH stretching of water, is present in all cases; below 1000 cm^{-1}, the spectra present a broad-saturated band related to the complex Al-O vibrations of alumina film (not shown in this figure). Nevertheless, the more interesting bands for the purpose of this work are those located between 1600 and 1100 cm^{-1}; they are characteristic of each sample and indicate the presence of the dopant anionic species inserted in the alumina matrix during the anodization process [27-29]. The partially resolved strong bands centered at 1130 cm^{-1} and 1145 cm^{-1} are related to the presence of sulfates and phosphates in the corresponding samples, while the pair of unresolved bands centered at 1547 cm^{-1} and 1465 cm^{-1} indicate the presence of oxalate anions. These last bands are assigned to the asymmetric and symmetric stretching of carboxilate anions, and the difference in their wave numbers suggests a bridging bidentated coordination of the oxalate groups with the aluminum cations [30,31].

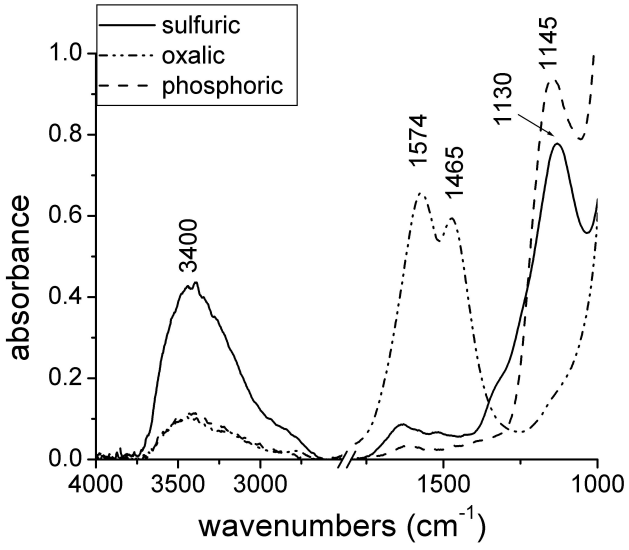

FIGURE 2. Infrared spectra of substrate-free films of: (—) sulfuric; (—· ··) oxalic; and (- - - -) phosphoric anodic aluminas.

4.2. Thermal analysis

Figures 3a, 3b present the TG curves of sulfuric and oxalic anodic aluminas; a similar multi-step mass-loss process is observed in both curves, but with quantitative differences (see Table I). Figure 3c presents the TG curve of the phosphoric alumina, which show a different profile. For all TG curves, the mass loss between room temperature and 400°C is attributed to a dehydration process involving both absorbed and coordinated water (region i). The absolute values of the mass loss (5.7% for sulfuric, 4.2% for oxalic and 1.2% for phosphoric alumina) may be assumed to be an indication of differences in the hydrophilic character of each sample. In a similar way, between 400 and 700°C, all samples present a continuous mass loss which is associated with a dehydroxilation process (region ii).

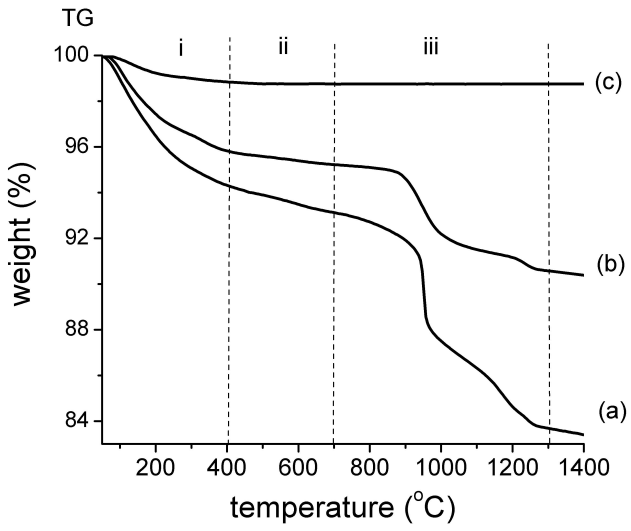

FIGURE 3. TG traces of: (a) sulfuric anodic alumina; (b) oxalic anodic alumina, and (c) phosphoric anodic alumina. Indicate (i) dehydratation, (ii) dehydroxilation process, and (iii) thermal decomposition of the dopant species present in anodic aluminas.

TABLE I. Transformation temperatures of the anodic aluminas.

Crystalline phase of AAO	Onset point °C DTA			Onset point °C DTG		
	Sulfuric	Oxalic	Phosphoric	Sulfuric	Oxalic	Phosphoric
transition aluminas	890	848	830	907	870	—-
$\alpha-Al_2O_3$	1223	1209	1368	1237	1210	—-

TABLE II. Mass loss from the TGA curves (sulfuric, oxalic and phosphoric aluminas).

Anodic Alumina	Mass-loss (%) (RT-400°C)	Mass-loss (%) (400-700°C)	Mass-loss (%) (700-1400°C)	Residual mass (%)
sulfuric	5.68 (H_2O)	1.19 (OH)	9.84 (SO_2)	83.29
oxalic	4.17 (H_2O)	0.60 (OH)	4.92 (CO_2)	92.45
phosphoric	1.15 (H_2O)	0.09 (OH)	—-	98.76

Above 700°C, the behavior of sulfuric and oxalic aluminas is clearly different from that of phosphoric aluminas. In the case of sulfuric and oxalic aluminas, two well defined and characteristic mass-loss events are observed around 800-1100°C and 1150-1300°C, which are associated with the thermal decomposition of the dopant species (sulfate or oxalate groups) present in these aluminas (region iii) [23,24]. The evolved decomposition products were identified as SO_2 for sulfuric alumina and CO_2 for oxalic alumina, using a quadrupole mass spectrometer coupled to the thermal analysis system [32]. On the other hand, above 700°C, the phosphoric anodic aluminas, Fig. 3c, present a plateau of thermal stability and no mass loss is found from them. This fact indicates that the phosphate groups do not thermally decompose but remain in the alumina matrix, which is a clear differentiation of its thermal behavior when compared to that of the sulfuric and oxalic aluminas.

The average P content of phosphoric anodic aluminas, obtained by X-Ray Fluorescence, was 4% in weight; from these data and the mass-loss values (see Table II) the following estimated composition for sulfuric, oxalic and phosphoric samples are proposed:

- Sulfuric anodic alumina: $(Al_2O_{2.77})_{100}(SO_4)_{19}(OH)_8 \cdot 39H_2O$
- Oxalic anodic alumina: $(Al_2O_{2.92})_{100}(C_2O_4)_6(OH)_4\ 26H_2O$
- Phosphoric anodic alumina: $(Al_2O_{2.88})_{100}(PO_4)_8(OH)_{0.1} \cdot H_2O$

In order to obtain the coefficient of the former empirical formulas, a classical stoichiometric calculation was used: the % mass loss of each species is divided by its corresponding molecular weight, and in this way a set of values for each kind of alumina is obtained. After that, all the values are divided by the lowest one, and the stoichiometric coefficients are then obtained. If necessary, these coefficients may be normalized in order to obtain a given value for a specific species (in our case we selected a value of 100 for the Al_2O_{3-x} content). The value of x for (Al_2O_{3-x}) was derived following the charge neutrality criterion.

From these empirical formulas it can be seen that, under the present experimental conditions, sulfuric alumina has a significantly higher concentration of dopant species, hydroxyl groups and water than the oxalic and phosphoric counterparts, indicating that this type of anodic alumina should have the highest hydrophilic character. In the same way, assuming the acidic character of some hydroxyl groups, it is to be expected that the sulfuric anodic aluminas would also have a higher acidic character than the oxalic and phosphoric aluminas. In addition, the analysis of these empirical formulas permits the quantification of an excess of oxygen (when compared with stoichiometric Al_2O_3), resulting from the incorporation of anionic species, which is close to 20% for sulfuric alumina and 7% for oxalic and phosphoric aluminas. Summarizing, a higher degree of hydrophilicity and acidity, together with a higher disorder or structural defects (due to their higher number of dopant species and oxygen excess) should be expected for sulfuric aluminas.

Figures 4a, 4b, and 4c present the DTA and DTG curves of the three types of aluminas. Going from room temperature to 400°C, all samples present the endothermal peaks due to dehydration processes, followed by exothermal peaks between 800-1100°C, related to the amorphous alumina matrix transformation into crystalline transition aluminas; and finally, an exothermal peak around 1250°C is associated with the formation of the α-Al_2O_3. Table I summarizes the crystalline transition temperatures for these samples. The specific crystalline phases formed will be discussed below, with the support of the corresponding X-ray diffractograms.

It is also important to note here that for all samples the onset temperature for forming the transition alumina phases is higher than for the amorphous aluminas obtained by chemical methods [33]. It seems that the presence of dopant anionic groups stabilizes the amorphous alumina matrix, extending its thermal existence interval. In other words, the formation of transition aluminas is hindered by the presence of anionic

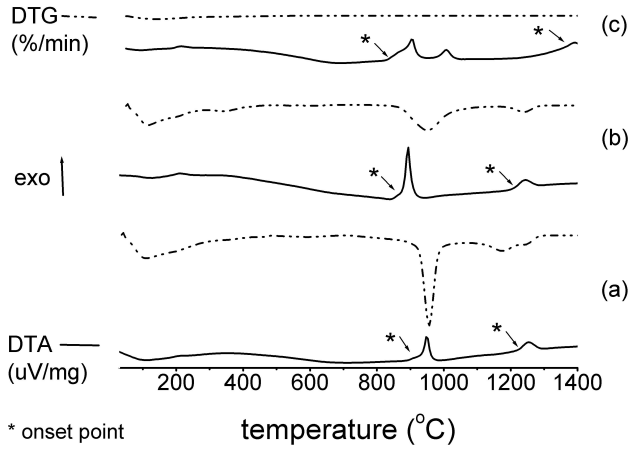

FIGURE 4. DTA(—) and DTG (····) traces of: (a) sulfuric anodic alumina, (b) oxalic anodic alumina, and (c) phosphoric anodic alumina.

groups, and only when a sufficiently high temperature is reached does the phase change proceed.

An important feature of sulfuric and oxalic aluminas is that the crystalline transition and the thermal decomposition of the dopant anionic species are coupled processes. As can be seen by comparing the DTG and DTA curves, that onset point of exothermal peaks slightly precedes the mass loss related to the thermal decomposition of sulfates or oxalates (Table I). Immediately after the crystalline transition, the dopant sulfates and oxalates become unstable, and their thermal decomposition products evolve. Finally, the last exothermal peak, centered about 1250°C for sulfuric and oxalic aluminas, is related to the formation of the α-Al_2O_3. A minor mass loss is also observed at this temperature, indicating that residual amounts of sulfates or oxalates are eliminated again in a coupled way with the transition phase.

In the case of the phosphoric alumina, the exothermal events related to the formation of the crystalline phases have their own profile, showing three exothermal peaks between 800 and 1400°C. The first one starts around 830°C and is clearly related to the formation of transition alumina, while the last one centered at 1392°C should be related to the formation of α-Al_2O_3. A detailed assignment of these three peaks requires the support of XRD studies, which will be presented in the following section.

4.3. X-ray diffraction

In order to identify the crystalline transitions associated with the DTA exothermal peaks of the different anodic aluminas, an XRD study of the phases present in the samples, treated at selected temperatures, was carried out. The selection of the treatment temperature for each anodic alumina was obtained from its DTA curve. Thus, sulfuric samples were treated at 850, 1150 and 1400°C, oxalic at 800, 1100, and 1400°C and phosphoric at 700, 920, 1050 and 1450°C. The phases formed for each sample, after the thermal treatment, are shown in Table III.

TABLE III. Crystalline phases for thermal treated anodic aluminas.

Anodic Alumina	Transition temperature and crystalline phase	
sulfuric	850°C	amorphous
	1150°C	γ-Al_2O_3
	1300°C	α-Al_2O_3
oxalic	800°C	amorphous
	1100°C	δ-Al_2O_3
	1400°C	α-Al_2O_3
phosphoric	700°C	amorphous
	920°C	$\gamma + \delta$-Al_2O_3
	1150°C	$\delta + \theta$-Al_2O_3
	1450°C	α-Al_2O_3, $AlPO_4$

As expected, all the original samples were amorphous and crystallized around 900-1000°C, forming transition alumina phases. It is important to note that it was not possible to make a precise identification of the transition alumina phases present for each temperature, and so the proposed assignment was done looking for the greatest similarity between the PDF files and the experimental diffractograms. The formation of pure, stable α-Al_2O_3phase occurs around 1300°C for both sulfuric and oxalic anodic aluminas.

Once again, the distinctive behavior of phosphoric alumina is also shown by its diffractogram. The diffractograms taken after the first crystalline transition indicate the presence of a mixture of $\gamma + \delta$ Al_2O_3, which became $\delta + \theta$ Al_2O_3after the second transition temperature. Finally, after the last crystalline transition (1450°C), the α-Al_2O_3 dominates the diffractogram, but additional peaks appear, indicating the formation of crystalline $AlPO_4$ (Fig. 5). The thermal stability of phosphate anions and their strong interaction with the aluminum result in the persistence of these species in the alumina matrix even after the formation of crystalline phases.

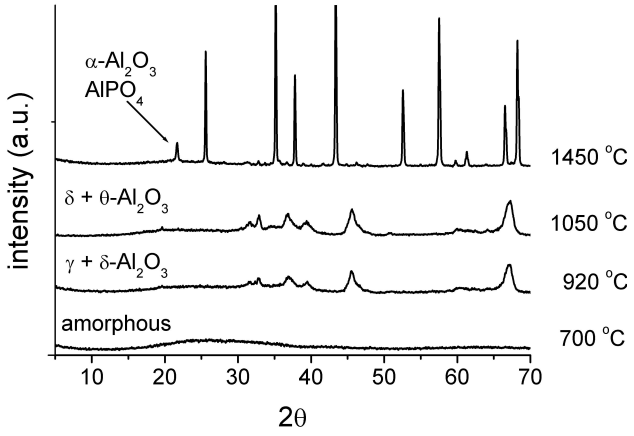

FIGURE 5. X-ray diffractograms of the phosphoric anodic alumina treated at different temperatures.

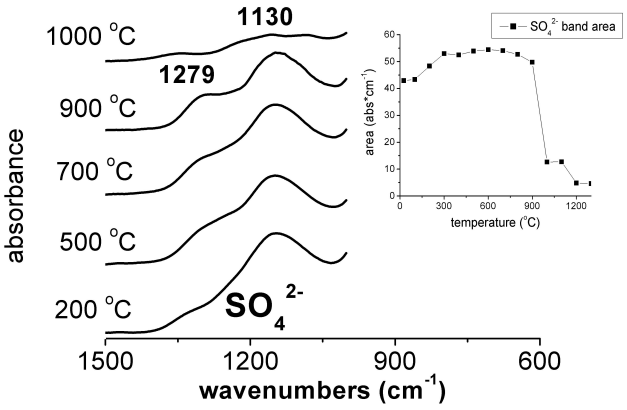

FIGURE 6. Infrared absorbance spectra of the sulfuric anodic alumina film at different temperatures. The inset shows evolution with temperature of the sulfuric band area.

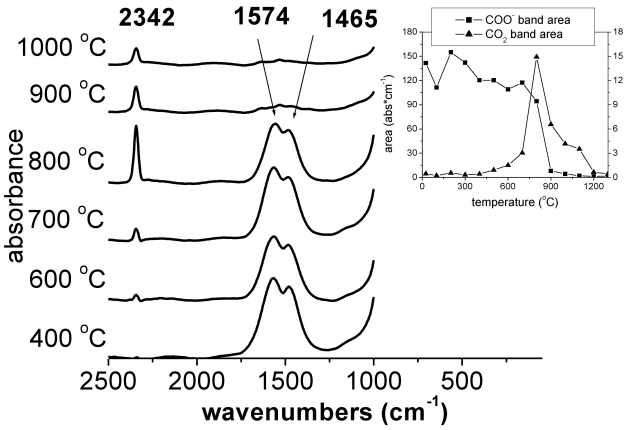

FIGURE 7. Infrared spectra of the oxalic aluminas between 400 and 1000°C. The inset shows evolution with the temperature of the area of the band related with oxalate anions.

4.4. Infrared spectra

In order to complete the information about the evolution of the dopant anionic groups with temperature, the infrared spectra of thermally heated substrate-free anodic alumina films were obtained. Figure 6 shows the 1500 to 1000 cm^{-1} interval of the infrared absorbance spectra of the sulfuric anodic alumina film at different temperatures. The band assignment of the room temperature spectrum is the same as in Fig. 2. The intensity of the band centered at 1130 cm^{-1}, assigned to the $\nu_3$vibrational mode of SO_4 [31], is almost constant until 800 °C, starts to decrease above 900°C, and almost disappears at 1200°C. This evolution is consistent with the mass loss observed in the TGA curve above 800°C, and supports the affirmation that this mass loss is due to the sulfate decomposition. The inset of Fig. 6 shows the evolution with the temperature of the whole area of the sulfate band. A careful observation of this 1130 cm^{-1} band points out the formation of a shoulder around 500°C, and the definition of a new maximum in 1279 cm^{-1} at 900°C. The splitting of the initial single band should be related to a change in the symmetry of the central sulfur atom [31], indicating that the coordination of the sulfates groups starts to change well before their thermal decomposition. That is, although the sulfate groups remain incorporated into the alumina matrix until 900°C, their coordination mode with the aluminum starts to change in the amorphous alumina phase 300°C, before the crystallization of the transition alumina and the subsequent thermal decomposition of sulfates.

Figure 7 shows the set of infrared spectra of the oxalic aluminas recorded between 2500 and 1000 cm^{-1} at different temperatures. Once again, in accordance with the mass loss of the corresponding TGA curve, the whole area of the oxalate bands (the inset of Fig. 7) shows a continuous decrease with temperature, and a drastic fall around 900°C, confirming that this loss is related to the removal of the oxalates. But now, the formation of a new band centered at 2342 cm^{-1} is also observed: this new band has its onset temperature around 500°C, its intensity increases with temperature between 500 and 800°C, strongly decreases at 900°C, and finally disappears around 1300°C. The combined evolution of the initial oxalate bands and the new one at 2342 cm^{-1} is presented in Fig. 7, in agreement with the previous report [24,34]. A band centered at 2342 cm^{-1} is associated [36] with the presence of carbon dioxide in monodentate coordination, and by extrapolation could be related, in this case, to the presence of monodentate carboxylate groups. Taking into account that the carboxilate groups initially had a bidentated coordination, it is possible to conclude that a large number of the oxalate groups change from a bridging bidentated to a monodentated coordination before their thermal removal as carbon dioxide. Once again, the coordination of the dopant anionic species starts to change in the amorphous oxalic alumina phase, clearly before their thermal decomposition.

Finally, Fig. 8a shows the set of infrared spectra of a substrate-free film of phosphoric aluminas treated from room temperature until 800°C; the mechanical fragility of these films makes them break above 800°C, and then the IR spectra of the film cannot be obtained above this temperature. Following the area of the phosphate band centered at 1145 cm^{-1}, Fig. 9 (triangles), it is observed to grow with the temperature. In order to confirm this unexpected trend beyond 800°C, a new set of samples treated between 850 and 1550°C was prepared using the standard KBr technique. Fig. 9 (circles) shows the evolution of the intensity of the 1145 cm^{-1} band above 800°C; due to the sample dilution with KBr, the initial intensity of this band appears now much weaker than in the film samples (triangles). Nevertheless the relative intensity keeps growing with temperature, particularly above 1400°C, that is, when the crystalline phase of $AlPO_4$ starts to form. Then, assuming that the amount of phosphates in the samples remains constant, it should be conclude that the growth of the band area is a consequence of the increase in crystallinity of the phosphate phase.

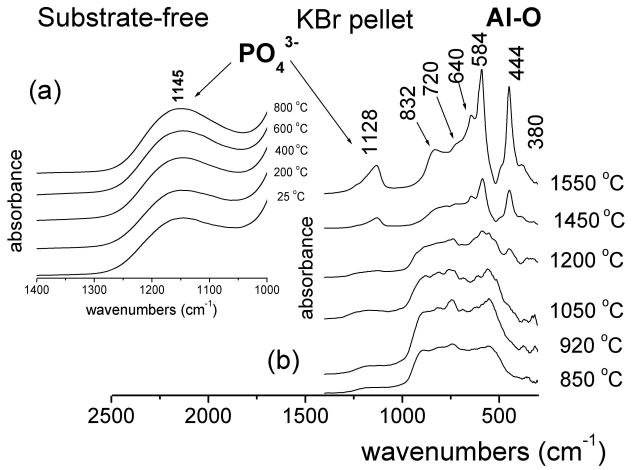

FIGURE 8. (a) Infrared spectra of a substrate-free film of phosphoric aluminas between room temperature and 800°C. (b) Infrared spectra of phosphoric aluminas samples prepared using the standard KBr technique.

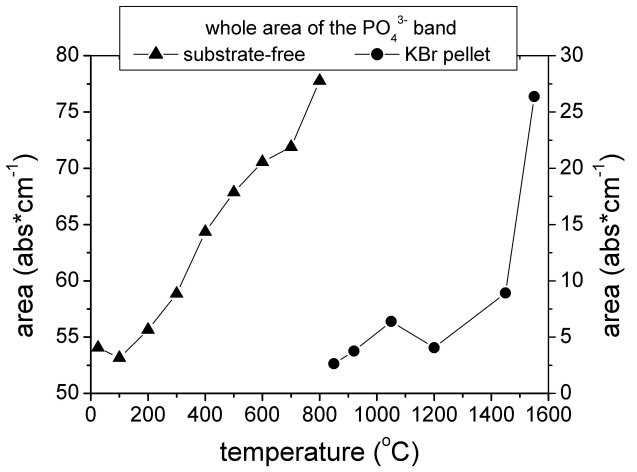

FIGURE 9. Evolution with the temperature of the phosphate band area. Substrate-free film (triangles), and KBr pellets (circles).

The spectra from the KBr pellets, Fig. 8b, also make it possible to observe the evolution of the Al-O vibration bands and even the formation of the $AlPO_4$. The almost unshaped band below 1000 cm^{-1} of the sample treated at 700°C represents the amorphous structure (not shown in this figure), while the broad, unresolved and complex band present between 850 and 1200°C is typical of the transition aluminas [37]. Finally, the set of the alfa-alumina sharp bands is easily identified above 1450°C [38], while the band at 1128 cm^{-1}, detected from 500°C on and reaching its highest definition at 1550°C, indicates the long thermal process leading to the formation of the $AlPO_4$ phase.

5. Conclusions

The systematic study of the thermal evolution of the sulfuric, oxalic and phosphoric porous anodic aluminas, makes it possible establish important differences in their physicochemical properties.

From the TGA curves and X-ray Fluorescence analysis, estimated empirical formulas were proposed for the sulfuric, oxalic and phosphoric aluminas obtained under the present experimental conditions. Using these empirical formulas, if follows that the sulfuric porous anodic alumina presents the highest hydrophilic character together with the highest structural disorder.

The thermal evolution of amorphous anodic aluminas is strongly affected by the dopant anionic species inserted in the alumina matrix during the anodization process. In all cases studied, the transformation temperature of the amorphous to transition alumina phase is about 300°C higher than that of amorphous aluminas obtained by chemical methods.

The anionic species inserted present a similar evolution with temperature in the case of sulfuric and oxalic aluminas, but not in the case of phosphoric alumina.

For the sulfuric and oxalic amorphous aluminas, the formation of the crystalline transition phases and the thermal removal of the anionic species are coupled processes. These transition alumina phases seem unable to support a high amount of coordinated dopant anionic species, which are then thermally decomposed and released from the alumina matrix.

The phosphoric anodic alumina presents a clearly different behavior, and the phosphate groups remain inserted into the alumina matrix even after the formation of transition and α-alumina phases. This difference is related to the thermal stability of the phosphates together with the high chemical affinity of the phosphates with aluminum.

The thermal evolution of the sulfates and oxalate infrared bands shows that the coordination of these species starts to change well before their thermal decomposition takes place. Around 400-900°C, the coordination mode of sulfates and oxalates experiences a progressive change, which in general terms result in the decreases in the coordination degree of the anionic species, as a previous step to their thermal decomposition and final release. In the case of the phosphoric alumina, the phosphates remain after the formation of transition alumina, but they start to segregate, forming an aluminum phosphate phase which coexists with the transition and the α-alumina matrix. The formation of the aluminum phosphate phase is detected by X-ray diffraction only above 1200°C, but the presence of a broad band in the infrared spectra at 1128 cm^{-1} at 900°C suggests that it could already be present, as low crystallinity aggregates at this temperature.

Acknowledgements

The authors would like to express their gratitude to A. Schindler and Nestzch Applications Laboratory for the identification of the thermal decomposition products of the anodic sulfuric and oxalic aluminas, to L. Baños from the Institute of Materials Research (UNAM) for the X-ray diffractograms, and to Patricia Girón from the Geology Institute (UNAM) for the X-ray fluorescence analysis. This work was supported by project 40507-F from CONACYT, Mexico.

1. J.W. Dingle, T.C. Downie, and C.W. Goulding, *Chem. Rev.* **69** (1969) 305.
2. G.E. Thompson, R.C. Furneaux, G.C. Wood, J.A. Richardson, and J.S. Goode, *Nature* **272** (1978) 433.
3. C.R. Martin, *Science* **266** (1994) 1961.
4. D. Rutkevitch *et al.*, *IEEET. Electron Devices* **43** (10) (1996) 1646.
5. A.P. Li, F. Müller, A. Birner, K. Nielsch, and U. Gösele, *J. Appl. Phys.* **84** (11) (1998) 6023.
6. K. Nielsch, J. Choi, K. Schwirn, R.B. Wehrspohn, and U. Gösele, *Nano Letters* **2** (7) (2002) 677.
7. G. Lajos Hornýak, *Characterization and optical theory of nanometal/porous alumina composite membranes*. Tesis, Doctor of Phylosophy in Chemistry Colorado State University, 1997.
8. Y.C. Sui *et al.*, **Mat. Res. Soc. Symp.** 633 (2001) A13.51.1.
9. X.Y. Zhang, L.D. Zhang, G.H. Li, and L.X. Zhao, *Mat. Sci. Eng. A* 308 (2001) 9.
10. T. Iwasaki, T. Motoi, and T. Den, *Appl. Phys. Lett.* **75** (14) (1999) 2044.
11. P.M. Paulus, E. Luis, M. Kröll, G. Schmid, and L.J. de Jongh, *J. Magn. Magn. Mater.* **224** (2001) 180.
12. Y. Lei, C.H. Liang, Y.C. Wu, L.D. Zhang, and Y.Q. Mao, *J. Vac. Sci. Technol. B* **19** (4) (2001) 1109.
13. G. Shi, C.M. Mo, W.L. Cai, and L.D. Zhang, *Solid State Commu.* **115** (2000) 253.
14. Y. Zhou, C. Shen, and H. Li, *Solid State Ionics* **146** (2002) 81.
15. J.D. Kein *et al.*, *Chem. Mater.* **5** (1993) 902.
16. Y.C. Sui, J.A. González-León, A Bermúdez, and J.M. Saniger, *Carbon* **39** (2001) 1709.
17. Y.C. Sui *et al.*, *J. Phys. Chem. B* **105** (2001) 1523.
18. A.B. Fuertes, *Carbon* **40** (2002) 1597.
19. O.K. Varghese, D. Gong, W.R. Dreschel, K. Gong, and C.A. Grimes, *Sensor. Actuat. B* **94** (2003) 27.
20. Y. Fujiwara and Y. Amao, *Sensor. Actuat. B* **89** (2003) 187.
21. Y. Yamamoto and N. Baba, *Thin Solid Films* **101** (1983) 329.
22. Y. Fukuda and T. Fukushima, *Bull. Chem. Soc. Jpn.* **53** (1980) 3125.
23. R. Ozao, M. Ochiai, N. Ichimura, H. Takahashy, and T. Inada, *Thermochim. Acta* **352/353** (2000) 91.
24. P.P. Mardilovich, A.N. Govyadinov, N.I. Mukhurov, A.M. Rzhevkii, and R. Paterson, *J. Membrane Sci.* **98** (1995) 131.
25. G. Partermarakis, K. Moussoutzanis, and J. Chandrinos, *Appl. Catalysis A: General* **180** (1999) 345.
26. G.E. Thompson and G.C. Wood, *Nature* **290** (1981) 230.
27. Y. Fukuda and T. Fukushima, *Bull. Chem. Soc. Jpn.* **57** (1980) 3125.
28. I. Farnan, R. Dupree, Y. Jeong, G.E. Thompson, G.C. Wood, and A.J. Forty, *Thin Solid Films* **173** (1989) 209.
29. H. Takahashi, F. Fujimoto, H. Cono, and M. Nagayama, *J. Electrochem. Soc.* **131** (8) (1984) 1856
30. J.M. Saniger, H. Hu, V.M. Castaño, and J. García-Alejandre, in: J.H. Adair, J.A. Casey, and S. Venigalla (Eds.), *Handbook on Characterization techniques for the solid-solution interface, The American Ceramic Society* (Ohio, USA, 1993) p. 169-175
31. K. Nakamoto, *Infrared and Raman spectra of inorganic and coordination compounds* (Wiley-Interscience publication Jhon Wiley & Sons, USA, 1986).
32. A. Schindler Netzch, Applications laboratory thermoanalytical section mass changes transformation energetics and evolved gas analysis of 3 porous anodic alumina samples, 820.057/03. 26 march 2003.
33. K. Wefers and C. Misra, *Oxides and hydroxides of aluminum*, Alcoa Technical Paper No. 19, Alcoa Laboratories, Pittsburgh, PA, 1987.
34. T. Gao, G. Meng, and L. Zhang, *J. Phys.: Condens. Matter.* **15** (2003) 2071.
35. P. Tarte, *Spectrochim. Acta A* **23** (1967) 2127.
36. C. Monterra, A. Zecchina, S. Coluccia, and A. Chiorino, *J. Chem. Soc. Faradays Trans.* **173** (1) (1977) 1544
37. J.M. Saniger, *Mater.Lett.* **22** (1995) 109.
38. C. Monterra and G. Magnacca, *Catal. Today* **27** (1996) 497.